Light scattering from liquid crystal director fluctuations in steady magnetic fields up to 25 tesla

Pavan K. Challa, O. Curtiss, J. C. Williams, R. Twieg, J. Toth, S. McGill, A. Jákli, J. T. Gleeson, and S. N. Sprunt

Phys. Rev. E **86**, 011708 — Published 23 July 2012

DOI: 10.1103/PhysRevE.86.011708

Light scattering from liquid crystal director fluctuations in steady magnetic fields to 25 Tesla

Pavan K. Challa,[1,*] O. Curtiss[2], J. C. Williams[3], R. Twieg[3], J. Toth[4], S. McGill[4], A. Jákli[5], J. T. Gleeson,[1] S. N. Sprunt[1]

[1]*Department of Physics, Kent State University, Kent, OH 44242*

[2]*Western Reserve Academy, Hudson, OH 44236*

[3]*Department of Chemistry, Kent State University, Kent, OH 44242*

[4]*National High Magnetic Field Laboratory, Tallahassee, FL 32310*

[5]*Chemical Physics Interdisciplinary Program and Liquid Crystal Institute, Kent State University, Kent, OH 44242*

ABSTRACT

We report on homodyne dynamic light scattering measurements of orientational fluctuation modes in both calamitic and bent-core nematic liquid crystals, carried out in the new split-helix resistive magnet at the National High Magnetic Field Laboratory. The relaxation rate and inverse scattered intensity of director fluctuations exhibit a linear dependence on field-squared up to 25 Tesla, which is consistent with strictly lowest order coupling of the tensor order parameter **Q** to field ($Q_{\alpha\beta}B_\alpha B_\beta$) in the nematic free energy. However, we also observe evidence of field-dependence in certain nematic material parameters, an effect which may be expected from the mean field scaling of these quantities with the magnitude of **Q** and the predicted variation of **Q** with field.

I. Introduction

In July, 2011, the National High Magnetic Field Laboratory (NHMFL) commissioned a new split-helix resistive magnet (the Split Florida-helix [1]) for optical scattering experiments in steady fields to 25 Tesla. The magnet features four identical ports radially arranged at 90° intervals around the high field region. Fig. 1 displays a cutaway view of the magnet that shows two of these ports, each providing ±22.5° free-space angular access (in the horizontal plane perpendicular to **B**) and ±5.7° access (in vertical plane parallel to **B**) to the center of the vertical magnet bore. The port arrangement allows unprecedented flexibility in the choice of scattering geometries for high-field experiments in a plane normal to **B.** It also affords placement of lasers,

* ckumar@kent.edu

optics, mechanical positioning and detection equipment a safe distance from the high-field region, which is located at the center of a 32 mm vertical bore tube. The space constraints of this region are thus decoupled from all apparatus except the sample chamber itself.

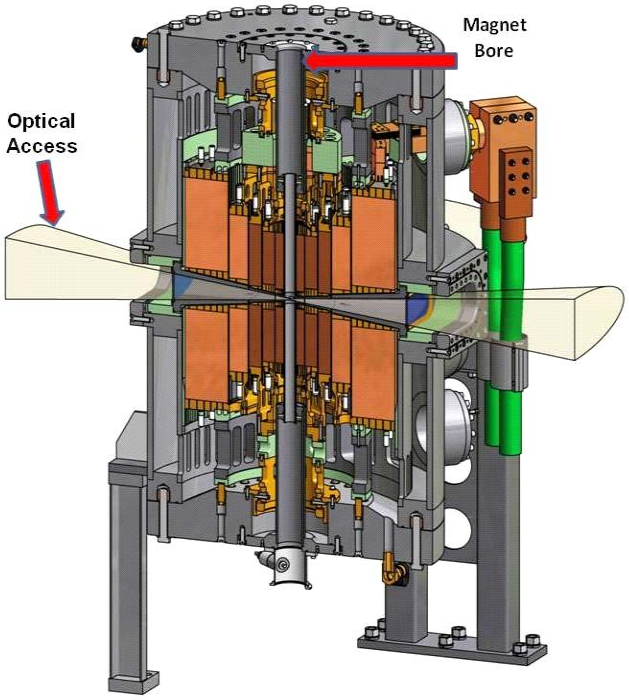

FIG. 1. A computer rendering of one half of the 25 Tesla Split Florida-helix at NHMFL.

As early users of this facility, we have sought to demonstrate its effectiveness in dynamic light scattering (specifically photon correlation spectroscopy or PCS) experiments on soft matter. Here we report an initial set of high-field measurements on both a standard rod-shaped (calamitic) and a more unconventional bent-core nematic (BCN) liquid crystal, which establish the practicality of high-quality, homodyne PCS studies in the Split Florida-helix. We show that the inverse amplitudes and the relaxation rates of optic axis (director) fluctuations in both nematics exhibit the theoretically expected B^2 dependence [2] in fields up to 25 Tesla. Our results also reveal evidence of a field-induced contribution to the Frank elasticity and viscosity for orientational fluctuations, which is anticipated from the mean field theory [3,4] that describes the scaling of these quantities with the nematic order parameter.

The capabilities of the Split Florida-helix should considerably expand the general scope of high-field studies of LCs, including quenching of director fluctuations and enhanced optical

birefringence in nematics [5]; magnetic field-induced phase transitions and related symmetry changes [6,7]; field effects on the phase diagram [8–12]; and the impact of field on pretansitional and critical phenomena [13–18], particularly in situations where large electric fields are impractical or deleterious to the sample. We hope that the results we present here, together with the extended data acquisition capabilities planned for the future, will inspire new users of NHMFL within the broader soft matter community.

II. Light scattering in the Split Florida-helix: Details of the set-up and application to liquid crystals

Our light scattering experiments in the Split Florida-helix were performed on the optical set-up pictured in Fig. 2 and presented schematically in Fig. 3. As shown in Fig. 2a, the laser (Coherent Compass series, model 315M, operating at 532 nm) and incident optics (spatial filter/collimator, Glan-laser polarizer, best-form f = 750 mm focusing lens) are mounted on a large non-magnetic optical table, which is assembled from one 8×4 ft and two 10×5 ft sections in a configuration that wraps around three sides of the magnet. In order to achieve the largest range of scattering angles, the laser light is directed into the magnet at an angle of approximately 20° with respect to center axis of the incident port. The main optical table also supports a 12×5 ft platform, positioned above the magnet, from which various sample chambers may be lowered into the 32 mm vertical bore. On the opposite side of the magnet from the incident port, a cantilevered platform extends from the table toward the scattering port. This platform supports an array of detection optical trains that collect scattered light at fixed angles (θ_s) between 0° and 40°. Each train consists of a pinhole aperture (which selects the scattering vector **q** and subtends approximately one coherence solid angle of the scattered light), an analyzer, and a multi-mode optical fiber onto which the illuminated volume of the sample is imaged by a separate imaging lens. The position of the fiber tips is finely adjustable to ensure peak collection efficiency at each angle. The detection optics, including the 5 m length of the collection fibers, are shielded from ambient room light by light-tight tubes.

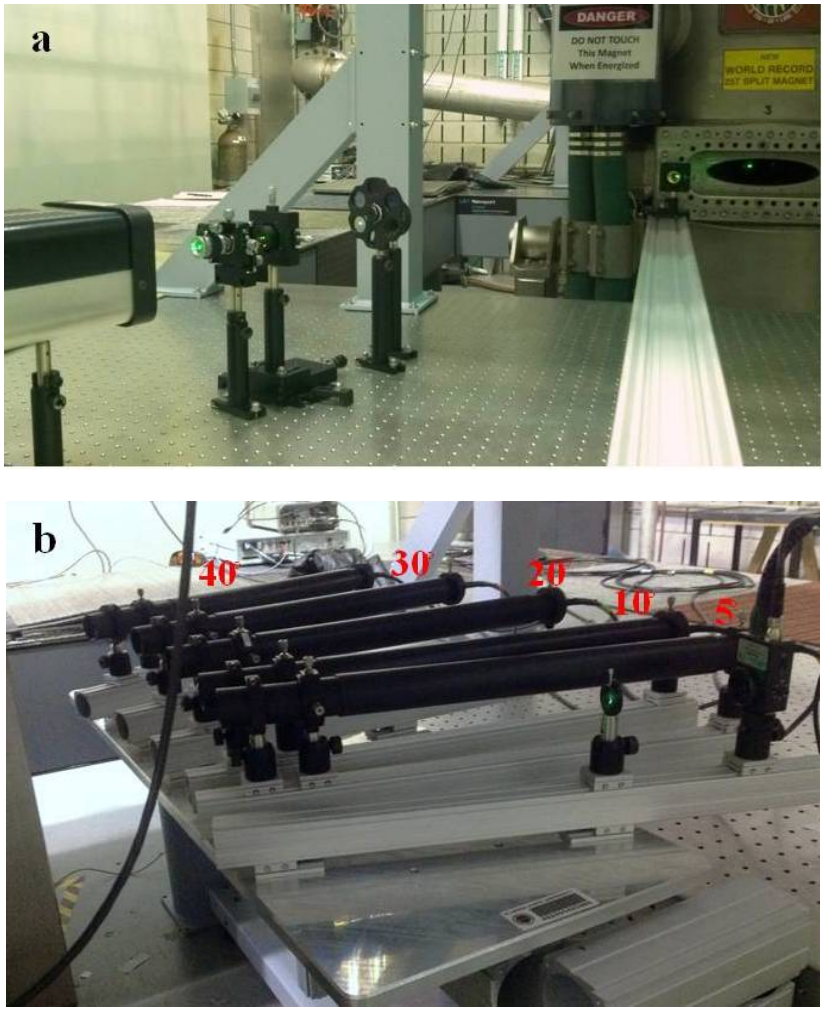

FIG. 2. (a) Incident optical layout. The focusing lens, incident port on the magnet, and the illuminated volume of the sample (at the center of the bore) are visible at right in the photo. (b) Collection optics platform, positioned on the opposite side of the magnet from (a), and showing optical trains at fixed scattering angles of 5°, 10°, 20°, 30°, and 40°. In the foreground at right is a photodiode used to monitor the (unscattered) laser power. All mechanical components are either non-magnetic or placed a sufficient distance from the bore, so that no movement was detected between zero and full field.

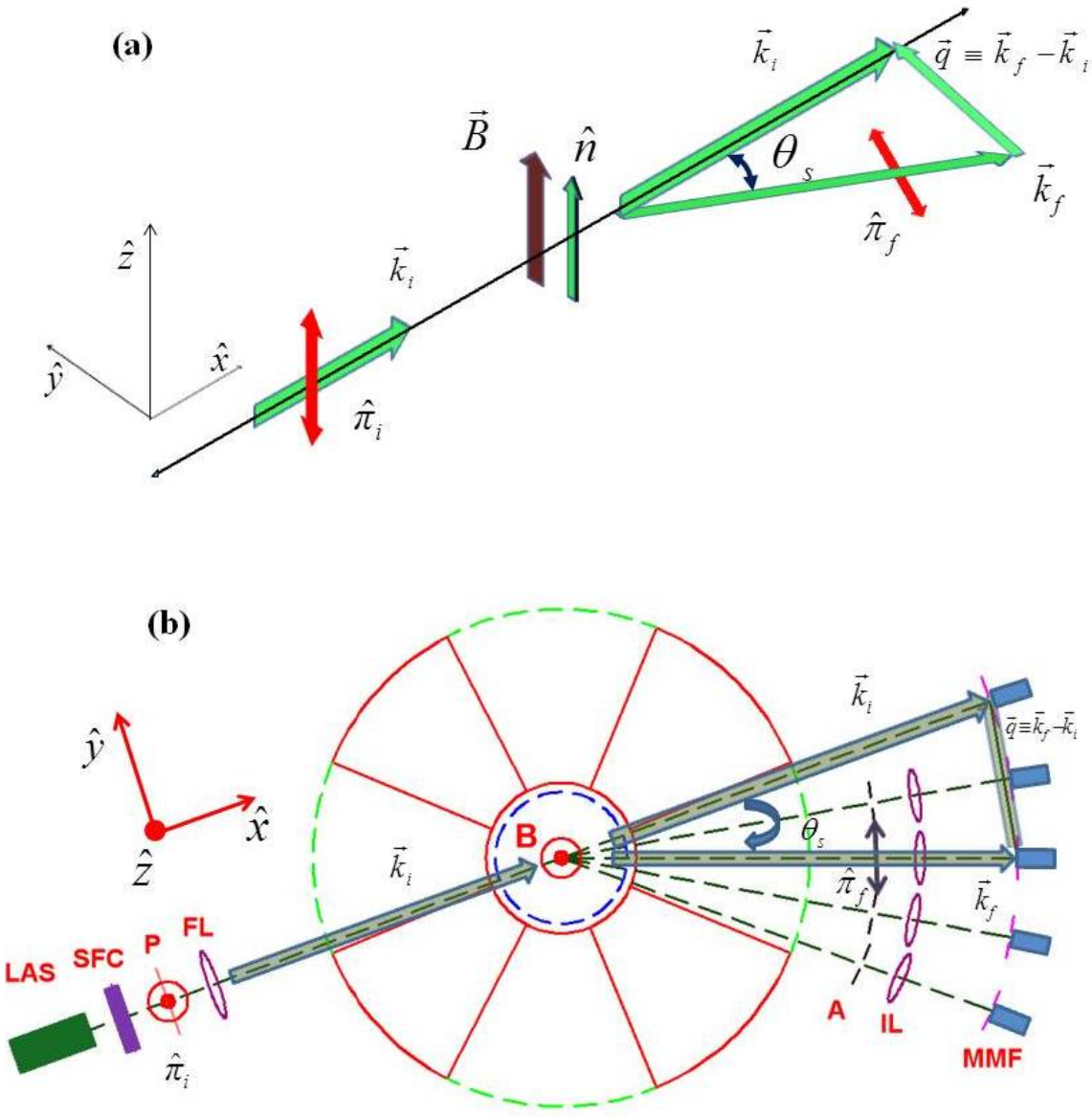

FIG 3. (a) Light scattering geometry to probe splay+twist fluctuations. (b) Schematic of optical layout for DLS with the Split Florida- helix. Laser (LAS), spatial filter/collimator (SFC), Glan-laser polarizer (P), focusing lens (FL), analyzer (A), imaging lens (IL), multimode fiber (MMF). θ_s is the lab scattering angle.

.

The collection fibers run several meters away from the scattering side of the magnet to a light-tight box just beyond the 10 gauss line. Inside the box, a selected fiber is plugged into a

module containing a laser line filter (1 nm FWHM) and a beam splitter that divides the scattered light into equal intensities, which fall onto two independent, magnetically-shielded photomultiplier detection modules (Hamamatsu, model HC120-08). The output signals from the PMTs pass through amplifier/discriminator circuits and then are cross-correlated in time by a digital electronic correlator (Correlator.com, model Flex2K-12Dx2). Cross-correlation was used to eliminate the effects of after-pulsing and dead-time in a single PMT on the measured correlation functions at delay times below ~1 μs. Sample temperature, magnetic field level, laser power, and correlation data are acquired simultaneously under Labview-based computer control.

With the current capability, auto-correlation data can be acquired from only two collection fibers (i.e., two scattering angles) at a time or, for pseudo cross-correlation, from a single angle. However, implementation of a 24 channel correlation system is planned for Fall, 2012. This system will enable parallel computation and live display of up to 12 simultaneous cross-correlations, resulting in a substantial operational economy for measurements in very high fields. (At 20 Tesla, the magnet uses 16.36 MW of power, while the standard energy budget for a typical experimental run of four 8 hr shifts is 200 MWh. The typical acquisition time for a single, high quality homodyne correlation function was 10 min.) The parallel system will support both correlation and photon history modes on all channels.

The two nematic liquid crystals (Fig. 4) used to demonstrate the capabilities of the present system are a standard commercially-available calamitic (4-pentyl-4'-cyanobiphenyl, abbreviated 5CB) and a bent-core compound (4-chloro-1,3-phenylene bis-[4'-(9-decenyloxy)benzoyloxy] benzoate, abbreviated ClPbis10BB [19]. The latter was synthesized and purified by J.C. Williams of the Department of Chemistry at Kent State. The liquid crystals were loaded into standard glass sandwich cells (EHC Co, Japan) that had a 10–15 μm gap for the sample and surface treatment for homogeneous planar alignment of the nematic director. Excellent uniaxial alignment was confirmed prior to the scattering measurements by polarizing microscopy. The isotropic to nematic transition temperatures were recorded as $T_{IN} = 35.0°\mathrm{C}$ (5CB) and 76.5°C (ClPbis10BB). The sample cells were placed inside a 31.5 mm diameter temperature-controlled and insulated oven, which has narrow horizontal slits for optical access. The oven was attached to a phenolic support rod, lowered from the fixed upper platform to the center of the magnet bore, and then rotated so that the laser light was incident at approximately

10° relative to sample cell normal. The sample and oven were secured in place by rigidly clamping the support tube to the upper platform. Proper vertical positioning of the oven (to 0.5 mm precision) was ensured using a reference mark on the support tube, whose placement matched a predetermined distance from the top platform to the center of the magnet. The sample's temperature was regulated to an accuracy of 0.01°C by a Lakeshore model 340 controller.

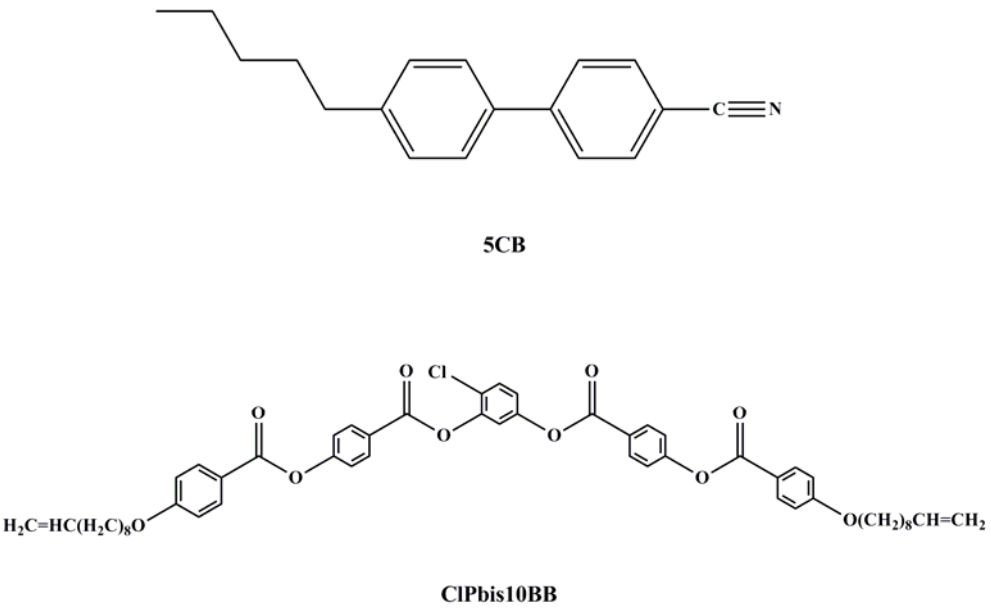

Fig. 4 Chemical structure of the nematic liquid crystals studied.

In the scattering geometry for our experiments (Fig. 3), the liquid crystal director **n** was oriented along the magnetic field **B** (vertical direction in the lab) and perpendicular to the (horizontal) scattering plane. The incident light polarization was vertical, and the depolarized scattered light was detected through horizontal analyzers at each scattering angle. This geometry corresponds to a simultaneous probing of pure elastic splay and twist distortions in the spectrum of thermal fluctuations of **n** [20]. In the presence of applied field **B**, their contributions to the scattered intensity I for scattering vector $\mathbf{q} = \mathbf{q}_\perp$ are [3],

$$I_\alpha = I_0 \frac{(\Delta\varepsilon)^2 k_B T \, G_\alpha}{K_\alpha q_\perp^2 + \Delta\chi B^2 / \mu_0} \tag{1a}$$

Here I_0 is the incident intensity, and we assume no absorption and negligible stray scattered light. The background count rate, recorded in the isotropic phase, was ~100 Hz or ~1% of the typical rate from the director scattering. The subscripts $\alpha = 1,2$ refer to splay or twist distortions, respectively, K_α are the associated Frank orientational elastic constants, $\Delta\varepsilon$ and $\Delta\chi$ are the optical dielectric and the diamagnetic anisotropies of the uniaxial nematic, and μ_0 is the permeability of space ($4\pi\times10^{-7}$ in SI units). The geometrical scattering factors G_α are given by [3]

$$G_1 = \frac{n_{\|}^2}{n_\perp^2}\left(\frac{\sin^2\theta_s}{n_\perp^2 + n_{\|}^2 - 2n_{\|}\sqrt{n_\perp^2 - \sin^2\theta_s}}\right)$$
$$G_2 = \frac{\left(n_\perp - \frac{n_{\|}}{n_\perp}\sqrt{n_\perp^2 - \sin^2\theta_s}\right)^2}{n_\perp^2 + n_{\|}^2 - 2n_{\|}\sqrt{n_\perp^2 - \sin^2\theta_s}} \qquad (1b)$$

where $n_{\|}, n_\perp$ are the refractive indices for light polarized parallel and perpendicular to the director.

Note that the denominator of Eq. (1a) contains an elastic term and a term due to diamagnetic coupling of **n** to the magnetic field, which is expressed to lowest order in the free energy density by the term $-\chi_{\alpha\beta}B_\alpha B_\beta/\mu_0$. (Here $\chi_{\alpha\beta} = \bar{\chi}\,\delta_{\alpha\beta} + \Delta\chi(n_\alpha n_\beta - \delta_{\alpha\beta}/3)$ is the diamagnetic susceptibility tensor of a uniaxial nematic, n_α are components of the director, $\delta_{\alpha\beta}$ is the Kronecker delta function, and we use the excellent approximation $\mu = \mu_0$ for diamagnetic liquid crystals.) Provided $\Delta\chi$ is positive (as is the case for both nematics studied), this term tends to suppress the fluctuation amplitude, and the scattered intensity is expected to decrease at fixed $\mathbf{q}_\perp$. In terms of the coordinate system in Fig. 3a, the scattering vector may be expressed as,

$$\mathbf{q}_\perp = \frac{2\pi}{\lambda_0}\left[\left(\sqrt{n_\perp^2 - \sin^2\theta_s} - n_{\|}\right)\hat{x} - \sin\theta_s\,\hat{y}\right] \qquad (2)$$

where λ_0 is the laser wavelength.

The director fluctuations in nematic liquid crystals are dominated by elastic and frictional (viscous) torques, and are therefore overdamped. According to the standard hydrodynamic theory of nematics, the relaxation rates for splay and twist fluctuations are,

$$\Gamma_\alpha = \frac{K_\alpha q_\perp^2 + \Delta\chi B^2/\mu_0}{\eta_\alpha} \tag{3}$$

where $\alpha = 1, 2$ and $\eta_1 = \gamma_1 - \frac{(\gamma_1 + \eta_b - \eta_c)^2}{4\eta_b}$, $\eta_2 = \gamma_1$ are combinations of the fundamental viscosities of a nematic fluid: γ_1 is a pure rotational viscosity (corresponding to simple rotation of **n**) and η_b, η_c are anisotropic Miesovicz flow viscosities of the nematic. In ordinary nematics, η_2 exceeds η_1 due to the "backflow" effect [21], whereby splay (or bend) distortions induce flow in the nematic fluid.

III. Results and Discussion

We measured the intensity correlation function for splay and twist director fluctuations at fixed scattering angles of 5°, 10°, 20°, 30° and 40° and magnetic fields up to 25 Tesla. Fig. 5 shows typical correlation data for 5CB recorded over 10 min at 32.5°C, 10° scattering angle, and for various field levels.

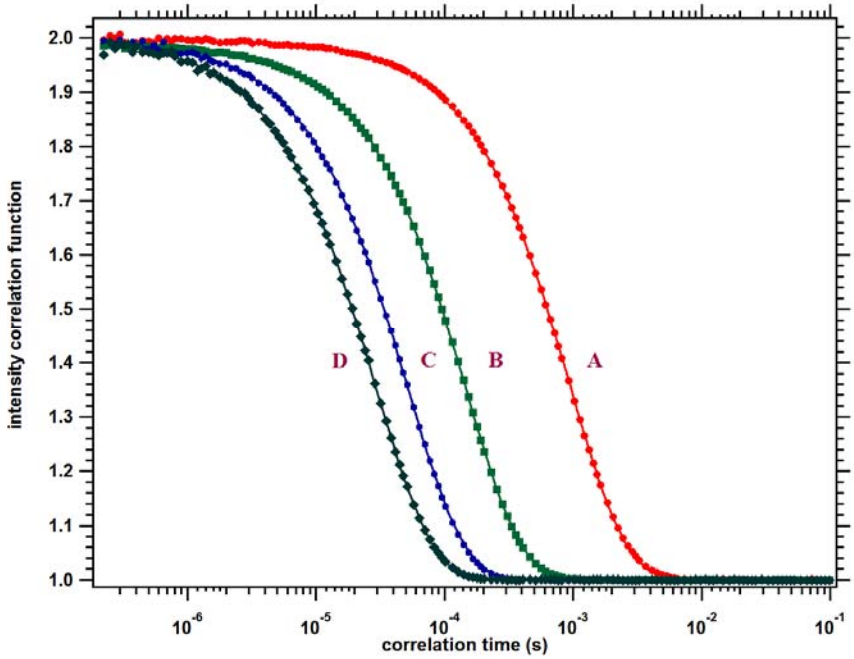

FIG. 5. Intensity correlation functions obtained on 5CB at $T_{IN} - T = 2.5°\text{C}$ and $\theta_s = 10°$ for various magnetic fields A (0T), B (11.2T), C (19.4T), D (25T). Dots represent the correlation data and lines correspond to fits described in the text.

Two features in these data are notable. First the quality of the homodyne signal is good; the correlation amplitude to baseline ratios exceed 0.97. Second, the relaxation rate Γ of the fluctuations increases (the decay time shifts to lower values) as the field *B* increases, as expected from Eq. (3) with $\Delta\chi > 0$.

Comparable data for the bent-core nematic ClPbis10BB at T = 70°C and $\theta_s = 10°$ are displayed in Fig. 6. The same comments just noted also apply here; however, the director mode relaxation rates are ~10^2 times smaller, in agreement with the much higher orientational viscosities η_1, η_2 reported previously [20]. The correlation baseline for these slower fluctuations is somewhat noisy; this flattens out over longer acquisition times.

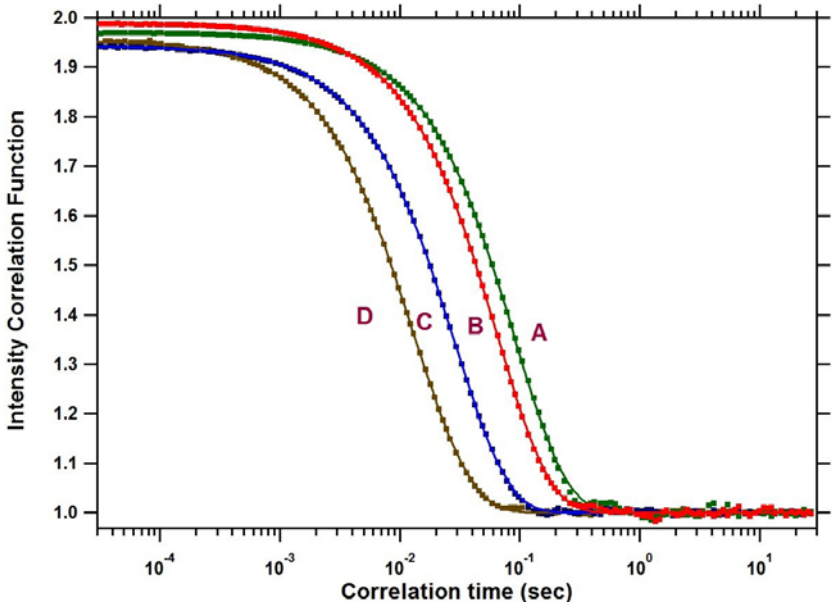

FIG. 6. Intensity correlation functions obtained on ClPbis10BB at $T_{IN} - T = 6.5°$ C and θ_s = 10°, for various magnetic fields A (5.9T), B (8.3T), C (14.4T), and D (22T). Dots are the correlation data and lines correspond to fits described in the text.

In principle, the correlation data in Figs. 5 and 6 should be fit to a combination of two exponential decays in time, corresponding to pure splay and twist director modes. However, the relaxation rates for these modes in thermotropic nematics are typically of the same order, so double exponential fits with two amplitudes and two relaxation rates often yield high parameter correlations and uncertainties. Since we are mainly interested in confirming the scaling of

parameters with B^2, which according to Eqs. (1a) and (3) should have the same form for splay and twist modes, we performed three parameter fits of the measured intensity correlation function $g(t)$ to the stretched exponential form,

$$g(t) = 1 + \{A \exp[-(\Gamma t)^{\beta}]\}^2 \tag{4}$$

The variable parameters are amplitude A, characteristic relaxation rate Γ, and stretching exponent β. (The squaring of the second term, which does not affect the qualitative behavior in this case, applies in the homodyne scattering limit.) The solid lines in Figs. 5 and 6 are the resulting fits.

For both samples, we find that the correlation decays are in fact nearly pure exponentials. The values of β range between 0.95 and 0.99, with the lowest value corresponding to the lowest θ_s ($\theta_s = 5°$) where, according to Eq. (1b), the twist fluctuations contribute strongly to the total scattering. Even here, β is close to 1 because the elasticity to viscosity ratios for splay and twist are within a factor of 2–3 of each other for 5CB [22]. For $\theta_s \geq 20°$ and using literature values of $n_{\|} = 1.68$, $n_{\perp} = 1.54$ at $T_{IN} - T = 2.5°$ C, we calculate $G_2 / G_1 \leq 0.12$ for the ratio of the twist to splay geometrical factors, so the scattering for larger θ_s is essentially due to pure splay, and a single exponential decay ($\beta \to 1$) should accurately describe $g(t)$. For ClPbis10BB, with $n_{\|} = 1.63$, $n_{\perp} = 1.53$ at $T_{IN} - T = 6.5°$ C, we obtain $G_2 / G_1 = 0.19$ for $\theta_s = 10°$, and again we expect and observe a nearly pure single exponential decay.

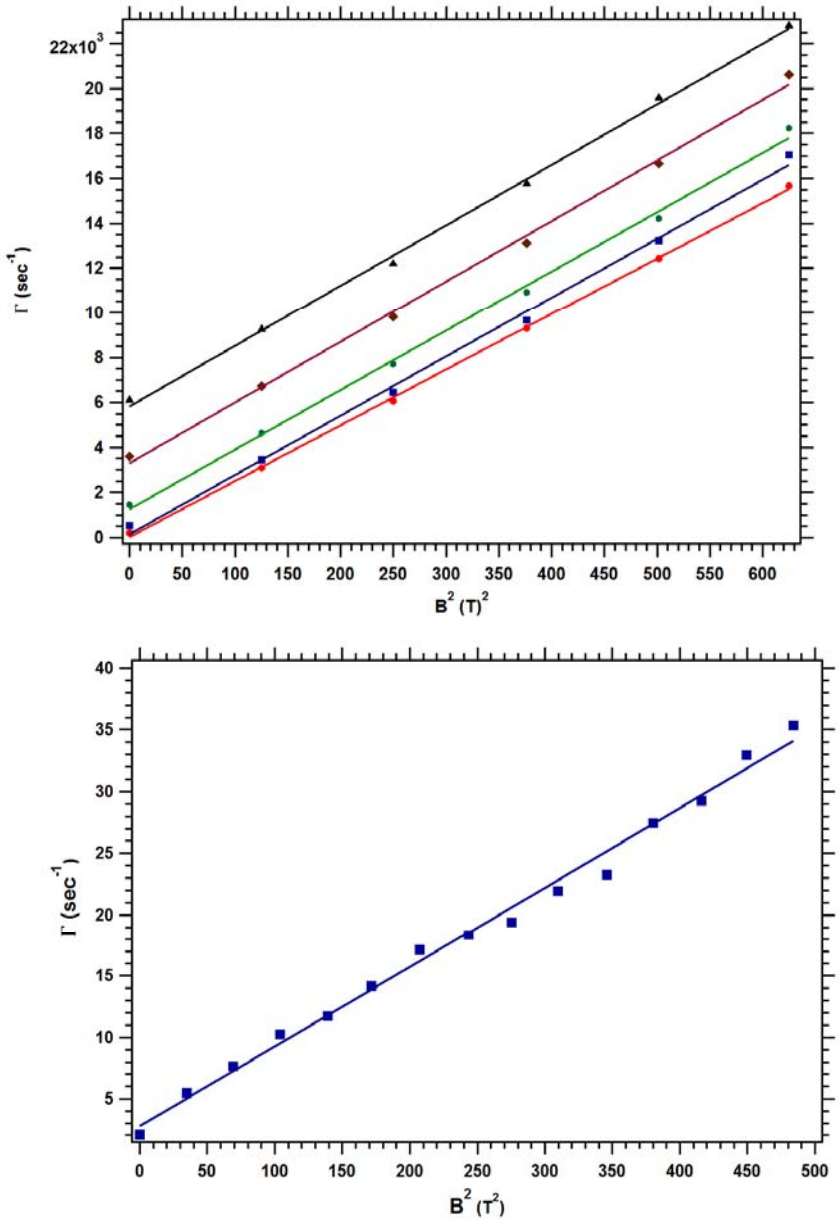

FIG. 7. Relaxation rate Γ of director fluctuations as a function field squared for 5CB (top) and ClPbis10BB (bottom) at fixed scattering angles θ_s. Dots are the experimental points and lines represent linear fits of Γ vs. B^2.

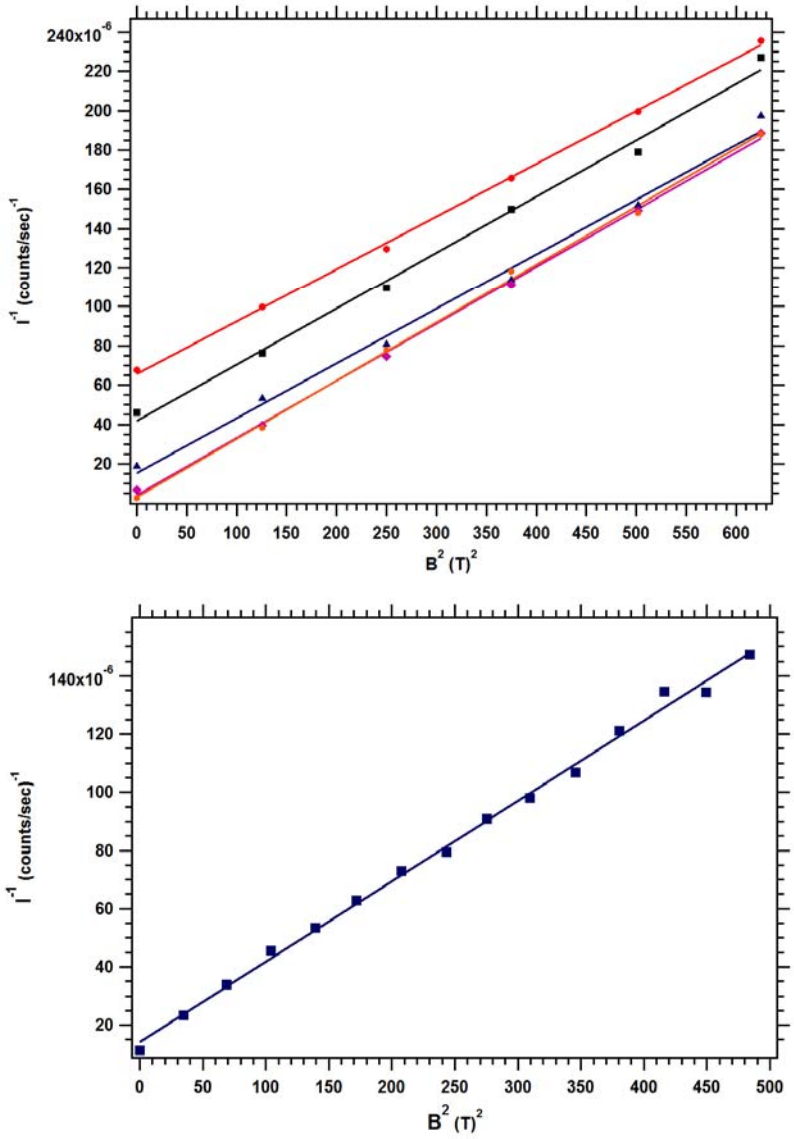

FIG. 8. Inverse scattered intensity vs. square of magnetic field for 5CB (top two plots) and C1Pbis10BB (bottom plot) at fixed scattering angles. Dots correspond to data and lines to linear fits.

Figs. 7 and 8 present representative plots of the B^2 dependence of the relaxation rate Γ [obtained from the fits to Eq. (4)] and the measured total inverse scattered intensity (I^{-1}) for 5CB and ClPbis10BB at temperatures of 32.5° and 70°C in the nematic phase, respectively, and for various scattering angles. These results clearly confirm the B^2 scaling of these quantities predicted by Eqs. (1) and (3) for fields up to 25 Tesla in both the calamitic and bent-core nematic compounds. No indication of coupling of field to the nematic order parameter tensor $Q_{\alpha\beta}$ beyond

the lowest order term, $Q_{\alpha\beta}B_\alpha B_\beta \sim B^2$, is detected in either material. A simple reliability check of our data can be made by using the average slope of the Γ vs B^2 data in Fig. 7 for 5CB, and literature values of the splay viscosity, to calculate $\Delta\chi$. We obtain $\Delta\chi = 1.6\times10^{-6}$, which is comparable to published values [23].

It is significant that we see no qualitative difference in the influence of field on fluctuations between the calamitic and bent-core nematics studied. ClPbis10BB and a number of other bent-core compounds exhibit an unusual "cybotaxis" (short-range smectic-like molecular order) that is apparently not associated with pretransitional behavior above a smectic phase [8,24,25], which is the usual and well-known basis for "cybotactic" behavior in nematics. The completely conventional scaling of I^{-1} and Γ with B^2 demonstrated in Figs. 7 and 8 suggests that the "cybotactic groups" in ClPbis10BB behave more like finite-sized smectic clusters (effectively "meta"-nematogens) than strongly fluctuating, pretransitional entities, in which case one could expect to observe some departure from simple B^2 dependence due to field-induced enhancement of the smectic correlations.

There is, however, one aspect of the field dependence of the data for Γ and I^{-1} that motivates a subtler interpretation of Eqs. (1) and (3). Namely, the data for 5CB at the five scattering angles studied (corresponding to $q_\perp$ between 2.0×10^6 and 8.3×10^6 m^{-1}) do not have the same slope, whereas superficially the theoretical expressions in Eqs. (1a) and (3) give *q*-independent slopes for Γ and I^{-1} versus B^2. As Fig. 9 reveals, the slopes $\frac{dI^{-1}}{dB^2}$ and $\frac{d\Gamma}{dB^2}$, obtained from the linear fits in Figs. 7 and 8, decrease and increase, respectively, with $q_\perp^2$. The variation is slight (5 – 7% over the full range of $q_\perp$), but apparently systematic. (The error bars represent plus or minus one standard deviation in the fitted slopes.)

One possible explanation for this behavior is a change with $q_\perp$ in the mixture of splay and twist contributions to the scattering. From Eq. (1a), for small $q_\perp$, we obtain $\frac{dI^{-1}}{dB^2} \propto \frac{\Delta\chi}{\mu_0}\left(\sum_\alpha G_\alpha\right)^{-1} = \frac{\Delta\chi}{\mu_0}$, since $G_1 + G_2 = 1$ from Eq. (1b). On the other hand for larger $q_\perp$

(corresponding to $\theta_s \sim 30-40°$), $G_1 \to 1, G_2 \to 0$, so again we have $\frac{dI^{-1}}{dB^2} \propto \frac{\Delta\chi}{\mu_0}$. Thus, the quantity $\frac{dI^{-1}}{dB^2}$, determined from our measurement of the total intensity, should be relatively insensitive to the mixture of modes. On the other hand, the slope of Γ versus B^2 (where Γ is obtained from a slightly stretched exponential fit to the correlation data) could increase with $q_\perp$ due to the crossover from mixed twist / splay to essentially pure splay from low to high θ_s: $\frac{d\Gamma_2}{dB^2} = \frac{\Delta\chi}{\mu_0\eta_2}$ is less than $\frac{d\Gamma_1}{dB^2} = \frac{\Delta\chi}{\mu_0\eta_1}$ because the splay viscosity η_1 is less than the twist viscosity η_2. This may account for the slight rise in $\frac{d\Gamma}{dB^2}$ in Fig. 9.

More interesting is the proposition that the observed dependence of the slopes on $q_\perp$ arises from implicit field-dependence of the elastic constants *K*, viscosities η, and the refractive indices affecting the value of $q_\perp$ in Eq. (2). According to mean field theory, the material parameters in Eqs. (1) – (3) scale with the magnitude *Q* of the nematic order parameter as [26] $K = K_0(Q^2 + \alpha_K Q^3)$, $\Delta\varepsilon = \varepsilon_a Q$, $\Delta\chi = \chi_a Q$, $n_\parallel^2 = \varepsilon_\parallel = \bar{\varepsilon} + \frac{2}{3}\varepsilon_a Q$, $n_\perp^2 = \varepsilon_\perp = \bar{\varepsilon} - \frac{1}{3}\varepsilon_a Q$, and $\eta = \eta_0(Q^2 + \alpha_\eta Q^3)$. Here ε_a and χ_a are the saturated dielectric and diamagnetic anisotropies, respectively, (the former at optical frequency), while K_0 and η_0 are the base elastic constant and orientational viscosity. $\bar{\varepsilon}$ is the average (isotropic) permittivity at optical frequency. To lowest order, the field dependence of *Q* in the nematic phase may be written as $Q = Q_0\left[1 + \alpha_Q (B/B^*)^2\right]$, where B^* is the critical field at the nematic-isotropic critical point and α_Q is a temperature dependent coefficient which is of order several tenths. Inserting these expressions into Eqs. (1) – (3), and expanding to order $(B/B^*)^2$, we get (suppressing the subscript α)

$$I^{-1} \approx \frac{\frac{K(Q_0)}{Q_0} q_{\perp 0}^2 + \left(\frac{\chi_a B^{*2}}{\mu_0} + K_0 Q_0^2 \alpha_K \alpha_Q q_{\perp 0}^2 + \frac{K(Q_0)}{Q_0} \frac{\varepsilon_a}{\varepsilon_0} k_0^2 \alpha_Q f_1(\theta_s) \right) \left(\frac{B}{B^*} \right)^2}{I_0 Q_0 \varepsilon_a^2 G_0 k_B T}$$

$$\Gamma \approx \frac{\frac{K(Q_0)}{Q_0} q_{\perp 0}^2 + \left[\frac{\chi_a B^{*2}}{\mu_0} + K_0 Q_0^2 \left(\alpha_K - \alpha_\eta \frac{1+\alpha_K Q_0}{1+\alpha_\eta Q_0} \right) \alpha_Q q_{\perp 0}^2 + \frac{K(Q_0)}{Q_0} \frac{\varepsilon_a}{\varepsilon_0} k_0^2 \alpha_Q f_2(\theta_s) \right] \left(\frac{B}{B^*} \right)^2}{\eta_0(Q_0)}$$

(5)

where $k_0 = 2\pi / \lambda_0$, $K(Q_0)$ and $\eta(Q_0)$ are the zero-field elastic constant and viscosity respectively, and $q_{\perp 0}$ is the value of $q_\perp$ using zero-field values of the refractive indices, $n_{\perp 0}$ and $n_{\| 0}$, in Eq. (2). For the case of splay (the dominant source of scattering except at the lowest value of θ_s studied), the functions f_1 and f_2 are: $f_1(\theta_s) = \frac{2}{3}\left[-\frac{1}{2} - \frac{3n_{\perp 0}^2}{2n_{\| 0}^2} + \frac{n_{\| 0}}{\sqrt{n_{\perp 0}^2 - \sin^2\theta_s}} + \frac{\sqrt{n_{\perp 0}^2 - \sin^2\theta_s}}{n_{\| 0}} \right]$ and $f_2(\theta_s) = \frac{1}{3}\left[1 + \frac{n_{\| 0}}{\sqrt{n_{\perp 0}^2 - \sin^2\theta_s}} - \frac{2\sqrt{n_{\perp 0}^2 - \sin^2\theta_s}}{n_{\| 0}} \right]$. Note that the leading terms in these expressions are constant in θ_s, and therefore simply combine with the constant term $\frac{\chi_a B^{*2}}{\mu_0}$ in Eq. (5).

Eq. (5) demonstrates that the slopes of I^{-1} and Γ vs B^2 depend on lab scattering angle θ_s (through terms involving $q_{\perp 0}^2$ and the functions f_1 and f_2). In particular, for $\alpha_K < 0$, the slope of I^{-1} should decrease with $q_\perp$; in fact, from measurements made on Q and the splay constant K_1 as a function of temperature, the parameter α_K was determined to be negative and as large in magnitude as ~0.7 for certain calamitic nematics [27]. Even so, standard estimates of B^* are quite large (~ 100 Tesla) [14],[28], and using such values in the expression for I^{-1}, one expects the variation of $\frac{dI^{-1}}{dB^2}$ with $q_\perp$ to be rather weak. Taking $n_{\perp 0} = 1.54$, $n_{\| 0} = 1.68$, $\frac{\varepsilon_a}{\varepsilon_0} \simeq 1$,

$\chi_a = 10^{-6}$, $K_0 Q_0^2 \simeq \dfrac{K(Q_0)}{Q_0} \simeq 10\,\text{pN}$, $\alpha_K = -0.7$, $\alpha_Q = 0.16$ [29], and the $-7\,\%$ change in $\dfrac{dI^{-1}}{dB^2}$ between $\theta_s = 0$ and $40°$ obtained from the straight line in Fig. 9, we estimate $B^* \simeq 80\,\text{Tesla}$. This value compares reasonably well with estimates of 100 Tesla based on Landau-deGennes mean field theory [28], but is significantly lower than values between 500 and 1000 Tesla calculated from Maier-Saupe or orientationally-averaged molecular pair correlation theories [14][28]. It is, however, well above the lower limit of ~20 Tesla previously established experimentally for a homolog of 5CB [30]. Clearly, it would be useful to extend measurements of $\dfrac{dI^{-1}}{dB^2}$ to significantly higher values of $q_\perp$, which can be reached using the wide optical access of the split Florida-helix, as well as perform more complete high-field scattering experiments on the bent-core compound ClPbis10BB and other reduced symmetry mesogens.

The $q_{\perp 0}^2$ dependence in the $\left(\dfrac{B}{B^*}\right)^2$ term for Γ in Eq. (5) involves an additional unknown parameter α_η, which evidently can compete with the effect of α_K. For this reason, and since a change in splay / twist mixture with $q_\perp$ plays a more important role in the value of $\dfrac{d\Gamma}{dB^2}$ (as discussed above), we will not discuss it further here.

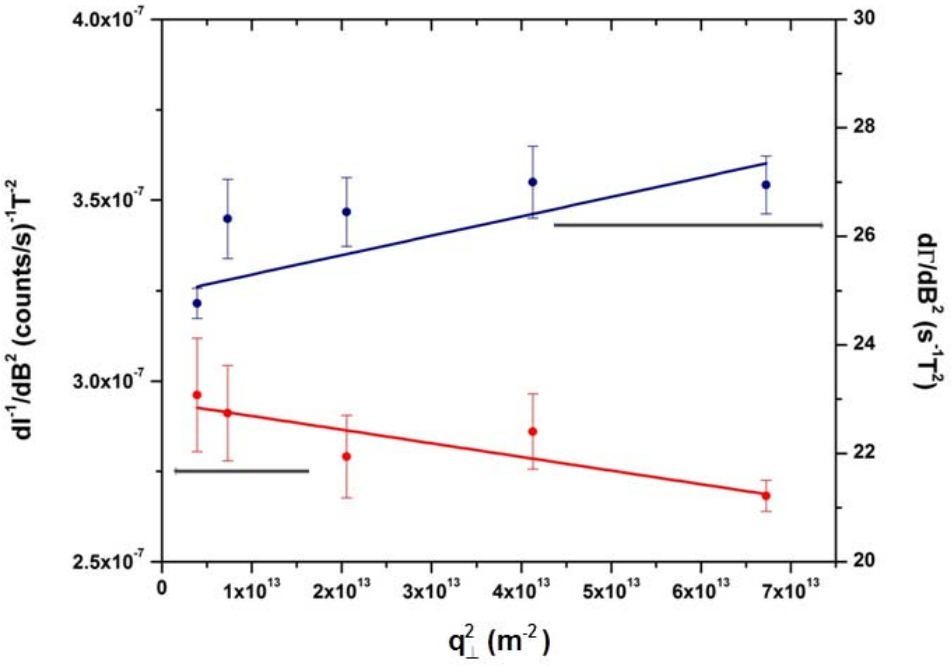

FIG. 9. The slopes $\frac{dI^{-1}}{dB^2}$ (in red) and $\frac{d\Gamma}{dB^2}$ (in blue), obtained from the fits to the data in Fig. 8 and plotted versus the zero field value of $q_{\perp}^2$ (denoted $q_{\perp 0}^2$ in Eq. (5)). The solid lines represent a linear dependence on $q_{\perp 0}^2$ and horizantal black arrows pointing towards the axes corresponding to the data.

IV. Conclusion

We demonstrated homodyne PCS over a wide range of scattering angles in the new Split Florida-helix high-field magnet. The predicted scaling with field of the scattered intensity and relaxation rate of director fluctuations was confirmed up to 25 Tesla in both a standard calamitic and a bent-core nematic liquid crystal. Utilizing the predictions of mean field theory, we developed evidence of the intrinsic field-dependence of material parameters and estimated the critical value of the field corresponding to the nematic-isotropic critical point in the calamitic compound. We believe that optical scattering in the Split Florida-helix will open up new opportunities for the study of structure, ordering and self-assembly, and fluctuations in soft matter under the influence of very high magnetic fields.

V. Acknowledgements

The authors acknowledge valuable assistance from W. Aldhizer and D. Semenov. We thank Prof. D. Allender for several useful conversations. Four of us (PC, AJ, JG, and SS) acknowledge support from the NSF under grant DMR-0964765. This work utilized the facilities of the NHMFL, which is supported by NSF cooperative agreement DMR-0084173, the State of Florida, and the US Department of Energy.

VI. References

[1] J. Toth, M. D. Bird, S. Bole, S. Gundlach, and J. O'Reilly, IEEE Transactions on Applied Superconductivity **20**, 660-663 (2010).

[2] Orsay Group, J. Chem. Phys. **51**, 816 (1969).

[3] P. G. de Gennes and J. Prost, *The Physics of Liquid Crystals, Second Edition* (Clarendon Press, Oxford, 1993), Chapter 3.

[4] E. F. Gramsbergen, L. Longa, and W. H. de Jeu, Physics Reports **135**, 195-257 (1986).

[5] B. Malraison, Y. Poggi, and E. Guyon, Phys. Rev. A **21**, 1012-1024 (1980).

[6] C. P. Fan and M. J. Stephen, Phys. Rev. Lett. **25**, 500-503 (1970).

[7] C. Rosenblatt, Phys. Lett. A **83** 221 (1981).

[8] O. Francescangeli, F. Vita, F. Fauth, and E. Samulski, Phys. Rev. Lett. **107**, 207801 (2011).

[9] W. Helfrich, Phys. Rev. Lett. **24**, 201-203 (1970).

[10] C. Rosenblatt, Phys. Rev. A **24**, 2236-2238 (1981).

[11] A. Sakamoto, K. Yoshino, U. Kubo, and Y. Inuishi, Jpn. J. Appl. Phys. **15**, 545-546 (1976).

[12] I. Lelidis and G. Durand, Phys. Rev. E **48**, 3822-3824 (1993).

[13] T. W. Stinson and J. D. Litster, Phys. Rev. Lett **25**, 503-506 (1970).

[14] P. J. Wojtowicz and P. Sheng, Phys. Lett. A 48 235 (1974).

[15] P. H. Keyes and J. R. Shane, Phys. Rev. Lett. **42**, 722-725 (1979).

[16] C. Rosenblatt, J. Phys. (Paris), Lett. **42**, 9-12 (1981).

[17] A. Primak, M. Fisch, and S. Kumar, Phys. Rev. Lett. **88**, 035701 (2002).

[18] D. Wiant, S. Stojadinovic, K. Neupane, S. Sharma, K. Fodor-Csorba, A. Jákli, J. T. Gleeson, and S. Sprunt, Phys. Rev. E **73**, 030703 (2006).

[19] K. Fodor-Csorba, A. Vajda, G. Galli, A. Jákli, D. Demus, S. Holly, and E. Gács-Baitz, Macromolecular Chemistry and Physics **203**, 1556-1563 (2002).

[20] M. Majumdar, P. Salamon, A. Jákli, J. T. Gleeson, and S. Sprunt, Phys. Rev. E **83**, 031701 (2011).

[21] F. Brochard, Molecular Crystals and Liquid Crystals **23**, 51-58 (1973).

[22] M. Cui and J. R. Kelly, Mol. Cryst. Liq. Cryst. **331**, 49 (1999).

[23] N. V. Madhusudana and R. Pratibha, Molecular Crystals and Liquid Crystals **89**, 249-257 (1982).

[24] S. H. Hong, R. Verduzco, J. C. Williams, R. J. Twieg, E. DiMasi, R. Pindak, A. Jákli, J. T. Gleeson, and S. Sprunt, Soft Matter **6**, 4819 (2010).

[25] C. Keith, A. Lehmann, U. Baumeister, M. Prehm, and C. Tschierske, Soft Matter **6**, 1704 (2010).

[26] David W. Allender, *Theoretical estimates for elastic properties of biaxial nematics*, International Meeting on Information Display, Digest of Technical Papers, Vol. **I**, pp.195-198, (2005).

[27] D. W. Berreman and S. Meiboom, Phys. Rev. A **30**, 1955 (1984).

[28] J. Shen and C.-W. Woo, Phys. Rev. A **24**, 493 (1981).

[29] D. Allender, private communication unpublished.

[30] C. Rosenblatt, Phys. Rev. A **25**, 1239 (1982).